Available online at www.sciencedirect.com
SCIENCE DIRECT®
Journal of Computational Physics 215 (2006) 274–297
JOURNAL OF COMPUTATIONAL PHYSICS
www.elsevier.com/locate/jcp

Spectral/*hp* penalty least-squares finite element formulation for the steady incompressible Navier–Stokes equations

V. Prabhakar *, J.N. Reddy

Department of Mechanical Engineering, Texas A&M University, College Station, TX 77843-3123, USA

Received 27 January 2005; received in revised form 4 August 2005; accepted 27 October 2005
Available online 19 December 2005

Abstract

In this paper, we present spectral/*hp* penalty least-squares finite element formulation for the numerical solution of steady incompressible Navier–Stokes equations. The continuity equation is treated as a constraint on velocity field and the constraint is enforced using the penalty method, which is equivalent to replacing the pressure variable p with $p^n = p^{n-1} - \gamma(\nabla \cdot \mathbf{u})$, where $\mathbf{u}$ is the velocity field, γ is the penalty parameter and superscript 'n' is non-linear iteration number. The modified Navier–Stokes equations are expressed as an equivalent set of first-order equations by introducing vorticity–dilatation or stresses as additional independent variables and the least-squares method is used to develop the finite element model. High-order basis functions are used to construct the discrete model. Unlike other penalty finite element formulations, equal order integration is used for all terms of the coefficient matrix. Schur complement method is used and all interior element degrees of freedom are condensed out and interface degrees of freedom are solved either by direct solver (banded Cholesky factorization) or iterative solver (preconditioned conjugate gradient). Present formulation produces very accurate results for even very low penalty parameters (10–40). In this way present formulation (and implementation) fixes perennial problem of bad conditioning of coefficient matrix associated with penalty formulations. Proposed formulation is verified using the exact solution of Kovasznay flow. Numerical results are also presented for a number of two-dimensional benchmark problems, e.g., 2D lid-driven cavity flow, flow over a backward-facing step, steady flow past a circular cylinder, and 2D flow past a large circular cylinder in a channel. Finally, the proposed formulation is extended to coupled velocity–temperature problems, and buoyant flow inside a square enclosure is solved to test the penalty least-squares finite element model developed herein.

Keywords: Penalty method; Spectral methods; *hp* Methods; Least-squares method; Viscous incompressible flow

1. Introduction

The past two decades have witnessed a great deal of progress in the area of computational fluid dynamics. A large number of methods have been proposed for the numerical solution of the Navier–Stokes equations

* Corresponding author.
E-mail addresses: prabhakarv@tamu.edu (V. Prabhakar), jnreddy@shakti.tamu.edu (J.N. Reddy).

0021-9991/$ - see front matter
doi:10.1016/j.jcp.2005.10.033

governing flows of viscous incompressible fluids. Direct discretization methods include finite difference and finite volume techniques, the finite element method using conformal and non-conformal elements, and spectral methods. The finite element method is considered to be the most effective method for solving solid mechanics problems but the method has not achieved the same level of acceptance in the context of fluid flow analysis.

The velocity–pressure finite element formulation of the incompressible Navier–Stokes equations has several disadvantages. When the standard weak form Galerkin formulation is used, the biggest problem to be faced is the use of compatible approximation spaces for the velocity field and pressure variable. The choice must be such that they satisfy the inf–sup (or LBB) condition [3,4]. The penalty finite element formulation [5] circumvents this problem. It also reduces one independent variable (pressure). However, the penalty formulation has its own disadvantages. In principle, a very high penalty parameter (10^8–10^{12}) is required to obtain accurate solutions. For high penalty parameters, the contribution from the viscous terms would be negligibly small compared to the penalty terms in the computer, and a trivial solution is obtained. This is termed as ''locking''. To circumvent locking and to obtain acceptable solution, underintegration (reduced integration) of penalty terms has been proposed [6]. The other problem with this formulation is inaccurate prediction of the pressure, which is calculated using equation

$$p = -\gamma(\nabla \cdot \mathbf{u}). \tag{1}$$

When C^0-continuous shape functions are used to interpolate velocities, pressure is discontinuous along element boundaries, and an averaging is needed to obtain *acceptable* pressure field [7]. However, pressure field computed in this manner is not very accurate; a very high penalty parameter is needed to obtain accurate pressure. For large values of penalty parameters, the condition number of the finite element coefficient matrix is very high and hence the convergence of iterative solvers is very poor.

First penalty based finite element formulation for the Navier–Stokes equations was proposed almost three decades ago and there have been subsequent improvements but it did not gain much popularity mainly because of ill-conditioning of coefficient matrix which renders iterative solvers ineffective. Recently, Bochov and Gunzburger [8] proposed least-squares based penalty formulation for Stokes equations but their study was mathematical and no numerical results were reported. Hasthaven and co-workers [9,10] have proposed spectral/hp penalty methods where they implement boundary conditions using this approach.

In this paper, we present spectral/hp penalty least-squares finite element formulation for fluid flow problems. We combine the idea of least-squares variational principles with penalty method. Least-squares formulations result in a symmetric positive-definite coefficient matrix, which can be solved using robust iterative methods like preconditioned conjugate gradient method. The least-squares formulation results in a minimization problem rather than a saddle point problem and the choice of elements is not subjected to the LBB condition. High-order element expansions are used to construct the discrete model, which does not experience locking. Equal-order integration is used for all the terms in this study. We implement iterative penalty method proposed by Gunzberger [11]. The best feature of present formulation is that it requires very small penalty parameter, 10–40 to yield very accurate solution. For such small penalty parameters, the coefficient matrix is better conditioned and convergence is not slow as in the traditional penalty finite element model. Due to the use of high-order expansions, we also obtain very accurate velocity as well as pressure fields. Thus, the disadvantages of the weak form penalty finite element model are overcome by the penalty least-squares finite element model.

We present this formulation as an alternative to the spectral/*hp* least-squares finite element formulation presented by Pontaza and Reddy [1,2] for steady and unsteady problems. In their formulation the divergence-free constraint on the velocity field is enforced directly through the least-squares functional, and pressure is retained as an independent variable. For unsteady problems, this approach seems to have disadvantages as the time-evolution of the pressure field is not well-behaved. It is believed that it lacks a strong pressure–velocity coupling. The present formulation avoids this problem altogether by eliminating pressure via Eq. (7).

The present paper is organized as follows. In Section 2, the penalty least-squares finite element model for the steady incompressible Navier–Stokes equations is presented. Numerical results are presented in Section 3. The spectral convergence is verified using the exact solution of the Kovasznay flow problem. First we present results for 2D lid-driven cavity problem at $Re = 10^4$ and compare the results with Jiang et al. [12]. Next, numerical results are presented for the two-dimensional flow over a backward-facing step and results are

compared with the benchmark solutions of Gartling [13] and Pontaza and Reddy [1]. Next, we consider flow past a circular cylinder at low Reynolds number and compare the predicted surface pressure distribution with experimental measurements of Grove et al. [14]. To test mass conservation rigorously, we solved 2D flow past a large circular cylinder in a channel. Lastly, in Section 4, we extend this formulation to velocity–temperature coupled problems and present results for buoyant flow inside a square enclosure and compare results with the benchmark solution of Davis et al. [15].

2. The incompressible Navier–Stokes equations

Notations: Let Ω denote an open bounded domain in $\mathbb{R}^n$, $n = 2$ or 3, having a sufficiently smooth boundary Γ. Throughout this paper, vectors will be denoted by boldface letters, e.g., $\mathbf{u}$, and tensors by underlined boldface capitals, e.g., $\underline{\mathbf{T}}$. We use the standard notation and definition for the Sobolev spaces $H^s(\Omega)$ and $H^s(\Gamma)$, $s \geqslant 0$, with corresponding inner products denoted by $(\cdot,\cdot)_{s,\Omega}$ and $(\cdot,\cdot)_{s,\Gamma}$. By $\mathbf{H}^s(\Omega)$ we denote the product space $[H^s(\Omega)]^n$; and $H^1_0(\Omega)$ denotes the space of functions from $H^1(\Omega)$ that vanish on the boundary Γ.

The steady Incompressible Navier–Stokes equations in dimensionless form can be written as follows:

$$(\mathbf{u}\cdot\nabla)\mathbf{u} + \nabla p - \frac{1}{Re}\nabla\cdot\left[(\nabla\mathbf{u}) + (\nabla\mathbf{u})^{\mathrm{T}}\right] = \mathbf{f} \quad \text{in } \Omega, \tag{2}$$

$$\nabla\cdot\mathbf{u} = 0 \quad \text{in } \Omega, \tag{3}$$

$$\mathbf{u} = \mathbf{u}^s \quad \text{on } \Gamma_u, \tag{4}$$

$$\hat{\mathbf{n}}\cdot\underline{\boldsymbol{\sigma}} = \mathbf{f}^s \quad \text{on } \Gamma_f, \tag{5}$$

where $\mathbf{u}(\mathbf{x})$ is the velocity vector, $\underline{\boldsymbol{\sigma}} = -p\underline{\mathbf{I}} + 1/Re[(\nabla\mathbf{u}) + (\nabla\mathbf{u})^{\mathrm{T}}]$ is the total stress, $p(\mathbf{x})$ is the pressure, $\mathbf{f}$ is a dimensionless force, $\hat{\mathbf{n}}$ is the outward unit normal on the boundary of Ω, $\mathbf{u}^s$ is the prescribed velocity on the boundary Γ_u, and $\mathbf{f}^s$ are the prescribed tractions on the boundary Γ_f, $\Gamma = \Gamma_u \cup \Gamma_f$ and $\Gamma_u \cap \Gamma_f = \emptyset$, and Re is the Reynolds number.

In the penalty method, pressure is eliminated from the Navier–Stokes equations using the following expression, which follows from the application of the penalty method to the Navier–Stokes equations with the divergence-free constraint (see [16–18]):

$$p = -\gamma(\nabla\cdot\mathbf{u}) \tag{6}$$

Gunzberger [11] proposed an iterative penalty method

$$p^n = p^{n-1} - \gamma(\nabla\cdot\mathbf{u}), \tag{7}$$

where n is the non-linear iteration number. An advantage of this method is that the value of penalty parameter needed to enforce the continuity constraint is equal to the square root of the one needed in the non-iterative penalty method [11]. This, in turn, results in a coefficient matrix with smaller conditioning number. In this study, we use the iterative penalty method.

Therefore, the problem becomes one of finding the velocity $\mathbf{u}(\mathbf{x})$ such that

$$(\mathbf{u}\cdot\nabla)\mathbf{u} - \gamma\nabla(\nabla\cdot\mathbf{u}) - \frac{1}{Re}\nabla\cdot[(\nabla\mathbf{u}) + (\nabla\mathbf{u})^{\mathrm{T}}] = \mathbf{f} - \nabla p^{n-1} \quad \text{in } \Omega, \tag{8}$$

$$\mathbf{u} = \mathbf{u}^s \quad \text{on } \Gamma_u, \tag{9}$$

$$\hat{\mathbf{n}}\cdot\underline{\boldsymbol{\sigma}} = \mathbf{f}^s \quad \text{on } \Gamma_f, \tag{10}$$

where n in the superscript $(n-1)$ is the non-linear iteration number. Since the solution at iteration $(n-1)$ is known, ∇p^{n-1} is known and therefore transferred to the right-hand side of the equation.

2.1. The velocity–dilatation–vorticity first-order system

To cast the second-order system (8)–(10) into a first-order system, we introduce the vorticity vector, $\boldsymbol{\omega} = \nabla\times\mathbf{u}$, and use the vector identity

$$\nabla\times\nabla\times\mathbf{u} = -\nabla^2\mathbf{u} + \nabla(\nabla\cdot\mathbf{u}).$$

We introduce another scalar independent variable dilatation, which is defined as

$$D = \nabla \cdot \mathbf{u}.$$

Then Eqs. (8)–(10) can now be replaced by an equivalent system of first-order equations. The problem now can be stated as one of finding the velocity vector $\mathbf{u}(x)$, dilatation $D(\mathbf{x})$, and vorticity $\boldsymbol{\omega}(\mathbf{x})$ such that

$$(\mathbf{u}\cdot\nabla)\mathbf{u} - \gamma\nabla D + \frac{1}{Re}\nabla\times\boldsymbol{\omega} = \mathbf{f} - \nabla p^{n-1} \quad \text{in } \Omega, \tag{11}$$

$$\boldsymbol{\omega} - \nabla\times\mathbf{u} = \mathbf{0} \quad \text{in } \Omega, \tag{12}$$

$$D - \nabla\cdot\mathbf{u} = 0 \quad \text{in } \Omega, \tag{13}$$

$$\mathbf{u} = \mathbf{u}^s \quad \text{on } \Gamma_u, \tag{14}$$

$$\boldsymbol{\omega} = \boldsymbol{\omega}^s \quad \text{on } \Gamma_\omega. \tag{15}$$

Typically $\Gamma_u \cap \Gamma_\omega = \emptyset$, i.e., if velocity is specified at a boundary, vorticity need not be specified there.

2.1.1. L_2 least-squares formulation

The least-squares functional of the problem can be set up by summing up the squares of the residuals of the new set of equations

$$\mathscr{J}(\mathbf{u}, D, \boldsymbol{\omega}; \mathbf{f}) = \frac{1}{2}\left(\left\|(\mathbf{u}\cdot\nabla)\mathbf{u} - \gamma\nabla D + \frac{1}{Re}\nabla\times\boldsymbol{\omega} - \mathbf{f} + \nabla p^{n-1}\right\|_0^2 + \|\boldsymbol{\omega} - \nabla\times\mathbf{u}\|_0^2 + \|D - \nabla\cdot\mathbf{u}\|_0^2\right). \tag{16}$$

Considering the homogeneous pure velocity boundary condition case, the least-squares principle for functional (16) can be stated as: find the velocity vector $\mathbf{u}(\mathbf{x})$, dilatation $D(\mathbf{x})$, and vorticity $\boldsymbol{\omega}(\mathbf{x})$ such that

$$\mathscr{J}(\mathbf{u}, D, \boldsymbol{\omega}; \mathbf{f}) \leqslant \mathscr{J}(\tilde{\mathbf{u}}, \tilde{D}, \tilde{\boldsymbol{\omega}}; \mathbf{f}) \quad \forall(\tilde{\mathbf{u}}, \tilde{D}, \tilde{\boldsymbol{\omega}}) \in \mathbf{X}, \tag{17}$$

i.e.,

seek $(\mathbf{u}, D, \boldsymbol{\omega})$ such that $\mathscr{J}(\mathbf{u}, D, \boldsymbol{\omega}; \mathbf{f})$ is minimized over $\mathbf{X}$,

where we use the space

$$\mathbf{X} = \left\{(\mathbf{u}, D, \boldsymbol{\omega}) \in \mathbf{H}_0^1(\Omega)\times H^1(\Omega)\times\mathbf{H}^1(\Omega)\right\}.$$

The variational problem (after linearization using Newton's method) corresponding to the least-squares principle is given by

$$\mathscr{B}((\mathbf{u}, D, \boldsymbol{\omega}), (\tilde{\mathbf{u}}, \tilde{D}, \tilde{\boldsymbol{\omega}})) = \mathscr{F}((\tilde{\mathbf{u}}, \tilde{D}, \tilde{\boldsymbol{\omega}})) \quad \forall(\tilde{\mathbf{u}}, \tilde{D}, \tilde{\boldsymbol{\omega}}) \in \mathbf{X}, \tag{18}$$

where

$$\begin{aligned}\mathscr{B}((\mathbf{u}, D, \boldsymbol{\omega}), (\tilde{\mathbf{u}}, \tilde{D}, \tilde{\boldsymbol{\omega}})) = {} & \int_\Omega \left((\mathbf{u}\cdot\nabla)\mathbf{u}_0 + (\mathbf{u}_0\cdot\nabla)\mathbf{u} - \gamma D + \frac{1}{Re}\nabla\times\boldsymbol{\omega}\right) \\ & \cdot\left((\tilde{\mathbf{u}}\cdot\nabla)\mathbf{u}_0 + (\mathbf{u}_0\cdot\nabla)\tilde{\mathbf{u}} - \gamma\tilde{D} + \frac{1}{Re}\nabla\times\tilde{\boldsymbol{\omega}}\right)\mathrm{d}\Omega + \int_\Omega (\boldsymbol{\omega} - \nabla\times\mathbf{u})\cdot(\tilde{\boldsymbol{\omega}} - \nabla\times\tilde{\mathbf{u}})\,\mathrm{d}\Omega \\ & + \int_\Omega (D - \nabla\cdot\mathbf{u})\left(\tilde{D} - \nabla\cdot\tilde{\mathbf{u}}\right)\mathrm{d}\Omega\end{aligned}$$

and

$$\mathscr{F}((\tilde{\mathbf{u}}, \tilde{D}, \tilde{\boldsymbol{\omega}})) = \int_\Omega (\mathbf{f} - \nabla p^{n-1} + (\mathbf{u}_0\cdot\nabla)\mathbf{u}_0)\cdot\left((\tilde{\mathbf{u}}\cdot\nabla)\mathbf{u}_0 + (\mathbf{u}_0\cdot\nabla)\tilde{\mathbf{u}} - \gamma\tilde{D} + \frac{1}{Re}\nabla\times\tilde{\boldsymbol{\omega}}\right)\mathrm{d}\Omega.$$

Let $\mathbf{X}_{hp}$ denote a finite-dimensional subspace of $\mathbf{X}$. Then the least-squares discretized model of the Navier–Stokes equations is defined by the following discrete variational problem: find $(u^{hp}, D^{hp}, \boldsymbol{\omega}^{hp}) \in \mathbf{X}_{hp}$ such that

$$\mathscr{B}((\mathbf{u}^{hp}, D^{hp}, \boldsymbol{\omega}^{hp}), (\tilde{\mathbf{u}}^{hp}, \tilde{D}^{hp}, \tilde{\boldsymbol{\omega}}^{hp})) = \mathscr{F}((\tilde{\mathbf{u}}^{hp}, \tilde{D}^{hp}, \tilde{\boldsymbol{\omega}}^{hp})) \quad \forall(\tilde{\mathbf{u}}^{hp}, \tilde{D}^{hp}, \tilde{\boldsymbol{\omega}}^{hp}) \in \mathbf{X}_{hp}. \tag{19}$$

2.1.2. Expansion bases

Having defined the finite element framework in terms of the penalty least-squares formulation, we need to choose proper basis functions to interpolate dependent variables. Almost all the penalty finite element implementations use low order expansions, linear or quadratic, and perform different order integration to integrate penalty terms and rest of the terms in the coefficient matrix. In this study, we use high-order interpolation functions that give p-convergence but computational work associated per degree of freedom is more compared to that of low order interpolation functions. One way to tackle the computational problem is to use expansion bases that are orthogonal. We use spectral bases that give exponential convergence and, the same time, satisfy orthogonality conditions. It is to be mentioned that all the variables are approximated using the same interpolation functions since there is no compatibility condition such as LBB condition in this formulation.

Nodal expansion: In the standard interval $\Omega_{st} = \{\xi \mid -1 < \xi < 1\}$ nodal expansions are defined as

$$\psi_i(\xi) = \frac{(\xi-1)(\xi+1)L_p'(\xi)}{p(p+1)L_p(\xi_i)(\xi-\xi_i)}. \tag{20}$$

In Eq. (20), $L_p = P_p^{0,0}$ is the Legendre polynomial of order p and ξ_i denotes the location of the roots of $(\xi-1)(\xi+1)L_p'(\xi) = 0$ in the interval $[-1,1]$. Nodal expansion follows discrete orthogonality, i.e., $\psi_p(\xi_q) = \delta_{pq}$. This property has been exploited during the calculation of conjugate gradient residual, which makes computations very fast. Details on the multidimensional construction of nodal expansions can be found in Ref. [19].

The integrals in Eq. (19) are evaluated using Gauss quadrature rules. In the computer implementation, Gauss–Lobatto–Legendre rule is used, which is imperative to exploit discrete orthogonality of nodal basis functions. This integration is not full integration still for the sake of fast numerical integration we use this. We would like to mention that this integration gives identically same results as full integration (Gauss–Legendre) gives and unlike in traditional penalty finite element formulation where coefficient matrix is almost singular and reduced integration is imperative to obtain acceptable solution. For details on standard finite element computer implementation, such as mapping $\bar{\Omega}_e \rightleftarrows \hat{\Omega}_e$, numerical integration in $\hat{\Omega}_e$, and assembly using the direct stiffness approach, see [16,17]. For linearization, we use Newton's method, details of which can be found in [21].

2.2. The stress based first-order system

To define the first-order velocity–stress system, 'scaled' stress tensor (symmetric part of velocity gradient tensor) is introduced

$$\underline{\mathbf{T}} = \left[(\nabla\mathbf{u}) + (\nabla\mathbf{u})^{\mathrm{T}}\right]. \tag{21}$$

Then Eqs. (8)–(10) can now be replaced by an equivalent system of first-order equations. The problem now can be stated as one of finding the velocity vector $\mathbf{u}(x)$ and stress tensor $\underline{\mathbf{T}}(\mathbf{x})$ such that

$$(\mathbf{u}\cdot\nabla)\mathbf{u} - \gamma\nabla\left[\frac{1}{2}\mathrm{tr}(\underline{\mathbf{T}})\right] - \frac{1}{Re}\nabla\cdot\underline{\mathbf{T}} = \mathbf{f} - \nabla p^{n-1} \quad \text{in } \Omega, \tag{22}$$

$$\underline{\mathbf{T}} - \left[(\nabla\mathbf{u}) + (\nabla\mathbf{u})^{\mathrm{T}}\right] = \underline{\mathbf{0}} \quad \text{in } \Omega, \tag{23}$$

$$\mathbf{u} = \mathbf{u}^s \quad \text{on } \Gamma_u, \tag{24}$$

$$\hat{\mathbf{n}}\cdot\underline{\mathbf{T}} = \mathbf{T}^s \quad \text{on } \Gamma_T. \tag{25}$$

Typically $\Gamma_u \cap \Gamma_T = \emptyset$, i.e., if velocity is specified at a boundary, and stress need not be specified there. The L_2 least-squares formulation and finite element model proceed in a similar manner as that described for the dilatation–vorticity based first-order system.

2.3. Implementation of boundary conditions

In general, in a given problem we have boundary conditions on the primary variables and/or secondary variables [16]. Boundary conditions on the primary variables can be implemented easily in the strong sense

by restricting the value of corresponding degree of freedom. Symmetry boundary conditions in 2D are $v = 0$ and $\omega = 0$ (at the wall $y =$ constant).

Boundary conditions on the secondary variables (typically, they involve derivatives of the primary variables) are imposed in a weak sense through the least-squares functional. For example, the outflow boundary condition, $\hat{\mathbf{n}} \cdot \tilde{\boldsymbol{\sigma}} = \hat{\mathbf{n}} \cdot (-p\mathbf{I} + (1/Re)\nabla\mathbf{u}) = 0$ is implemented by modifying the L_2 least-squares functional to be

$$\mathscr{J}(\mathbf{u}, D, \boldsymbol{\omega}; \mathbf{f}) = \frac{1}{2}\left(\left\| (\mathbf{u}\cdot\nabla)\mathbf{u} - \gamma\nabla D + \frac{1}{Re}\nabla\times\boldsymbol{\omega} - \mathbf{f} + \nabla p^{n-1} \right\|_0^2 + \|\boldsymbol{\omega} - \nabla\times\mathbf{u}\|_0^2 + \|D - \nabla\cdot\mathbf{u}\|_0^2 + \|\hat{\mathbf{n}}\cdot\tilde{\boldsymbol{\sigma}}\|_{0,\Gamma_{\text{outflow}}}^2 \right). \tag{26}$$

In the boundary term, pressure p is replaced by $(p^{n-1} - \gamma D)$. For long domains, the strong outflow boundary condition $p = 0$ also gives good results [1].

2.4. Solution of algebraic equations

In this study, we use both direct as well as iterative solvers. We use Schur complement method [22,19] and condense out all interior degrees of freedom. Fig. 9 shows one such mesh with interface nodes shown by square symbols and interior nodes shown by triangles. Since interior nodes of an element are not connected to other elements, coefficient matrix entries of corresponding degrees of freedom get contribution only from the nodes of that element and hence can be expressed in terms of interface nodes of that element. In this way, all interior degrees of freedom are eliminated and the system of equations is solved for interface degrees of freedom. Details of Schur complement can be found in [19,22]. While generating the mesh, one should number global interface degrees of freedom first, followed by global interior degrees of freedom. In addition, the global interior degrees of freedom should be numbered consecutively to maximize the benefit of this procedure.

The Schur complement method has twofold benefit. First, if coefficient matrix is stored, then one needs to store coefficient matrix corresponding to interface degrees of freedom. This saves tremendous amount of memory and one needs to solve for only the interface degrees of freedom. Second, conditioning number of new coefficient matrix is significantly lower than that of original matrix and iterative solvers converge faster [19]. To construct Schur complement, we need to invert elemental coefficient matrices which is computationally very cheap. Once Schur complement matrix is constructed, direct or iterative solvers can be used to solve this system. We note that Schur complement method can also be implemented in 'element by element' PCG method, where the global coefficient matrix is not stored (see [23] for details on 'element by element' solution algorithm). This is particularly desirable for large problems where even coefficient matrix corresponding to interface degrees of freedom requires large memory.

2.4.1. Direct solvers

Schur complement eliminates all interior degrees of freedom and therefore memory storage required to save coefficient matrix is significantly low and direct solvers can be used for relatively large problems. Given a SPD coefficient matrix, N_{dof} by N_{dof} with bandwidth B, banded Cholesky factorization is an effective direct solver provided $N_{\text{dof}} \gg B$. The amount of work required for this factorization is approximately $N_{\text{dof}}(B^2 + 3B)$ flops and N_{dof} square roots. We store only the non-zero lower triangular part in a $(B + 1)$ by N_{dof} array. At this point we caution the reader that because of round-off errors Cholesky factorization may not be stable (square-root of negative numbers may arise); see [20]. In particular, for high penalty parameters, Cholesky factorization may be unstable. But the present formulation requires very low value of penalty parameter and hence we did not face this problem.

2.4.2. Iterative solvers

For large problems, direct solvers are not a good choice both in terms of computer memory and CPU time. For SPD coefficient matrix, preconditioned conjugate gradient (PCG) methods are optimal choice. In this study we use Jacobi preconditioner as only diagonal entries of coefficient matrix are needed to be stored as opposed to other preconditioners which require partial or full storage of coefficient matrix.

2.5. Calculation of pressure

Unlike the non-iterative penalty method, in the iterative penalty method, pressure is calculated (actually updated) in every non-linear iteration through the following equation

$$p^n = p^{n-1} - \gamma D^n. \tag{27}$$

Thus no post-processing is needed in this formulation to compute pressure. Unlike penalty finite element formulations where pressure is not continuous, this formulation gives smooth and very accurate pressure field.

3. Numerical results

In this section, numerical results obtained with the penalty least-squares finite element model are presented for a number of benchmark problems. First, spectral convergence of the proposed algorithm is verified for both vorticity–dilatation and stress based least-squares finite element formulations. Next, results are presented for 2D lid-driven cavity flow, flow over a backward-facing step, and flow past a circular cylinder at low Reynolds number. To test mass conservation rigorously we solve 2D flow past a large circular cylinder in a channel. We use vorticity–dilatation based first-order system in this study because it carries lesser degrees of freedom compared to stress based first-order system and gives equally accurate results. We also investigate accuracy of the formulation with respect to the penalty parameter for these problems.

In this study, both direct and iterative solvers are used. All results presented are obtained using direct solver (banded Cholesky factorization) unless stated otherwise. Real world fluid mechanics problems are generally big in size requiring large number of degrees of freedom. For such problems direct solvers are not efficient because of both memory required and CPU time taken. Therefore, all problems are also solved using iterative solver (PCG), and PCG convergence histories are reported, which show that present formulation is free from ill-conditioning problem. Dilatation contours are presented for all problems apart from reporting L_2-norm of the residual of continuity equation (dilatation) as L_2-norm gives global picture only. The L_2-norm of the least-squares functional and other variables are defined as

$$\|\mathscr{J}\|_0 = \left[\frac{1}{2}\sum_{e=1}^{Nem}\int_{\Omega^e}\left(R_1^2 + R_2^2 + R_3^2 + R_4^2\right)\mathrm{d}\Omega^e\right]^{\frac{1}{2}},$$

$$\|D\|_0 = \left(\sum_{e=1}^{Nem}\int_{\Omega^e} D^2\,\mathrm{d}\Omega^e\right)^{\frac{1}{2}},$$

where R_i is residual of ith partial differential equation of the system and D is an independent variable (dilatation, vorticity, etc.). Some authors report square of these values. Nevertheless spectral convergence is important. L_2-norm of the residual should decay exponentially with p-level.

For all the problems considered in this paper, non-linear convergence is declared when the relative norm of the residual, $\|\Delta\mathbf{U}\|/\|\mathbf{U}\|$ is less than 10^{-3} unless mentioned, where $\mathbf{U}$ is the solution vector (includes all degrees of freedom at a node). Convergence of conjugate gradient is declared when L_2-norm of error is less than 10^{-6}.

3.1. Verification problem: Kovasznay flow

The benchmark problem to be used for the purpose of verification of the least-squares based finite element models is an analytical solution to the two-dimensional steady incompressible Navier–Stokes due to Kovasznay [24]. Domain of interest is $\bar{\Omega} = [-0.5, 1.5] \times [-0.5, 1.5]$. The solution is given by

$$u = 1 - \mathrm{e}^{\lambda x}\cos(2\pi y), \tag{28}$$

$$v = \frac{\lambda}{2\pi}\mathrm{e}^{\lambda x}\sin(2\pi y), \tag{29}$$

$$p = p_0 - \frac{1}{2}\mathrm{e}^{2\lambda x}, \tag{30}$$

where $\lambda = Re/2 - [(Re^2/4) + 4\pi^2]^{1/2}$ and p_0 is a reference pressure (an arbitrary constant).

Drichlet boundary conditions on velocities are specified using the exact solution given by Eqs. (28) and (29). The discrete system is linearized using Newton's method and resulting symmetric positive-definite (SPD) system of equations has been solved using the Choleski factorization. A uniform mesh of 64 quadrilateral elements is used for spatial discretization. Newton's convergence is declared when the relative norm of the residual is less than 10^{-10}. Penalty parameter used is 10^2 for which L_2-norm of the residual of continuity equation is below 10^{-12} for all p-levels used here and does not interfere with the spectral convergence.

Streamlines obtained with the present formulation for the Kovasznay flow are shown in Fig. 1(a). Fig. 1(b) contains dilatation contours. To verify spectral convergence, L_2-norm of least-square functional $\mathscr{J}$ and L_2 error of the velocity, pressure and vorticity fields are plotted against polynomial order in Fig. 2 for the dilatation–vorticity based first-order formulation. On logarithmic-linear scale we obtain almost straight line for all the variables verifying exponential decay with respect to the polynomial degree used.

Next, spectral convergence of stress based first-order system is verified. Fig. 3 shows that formulation achieves spectral convergence for all variables including pressure. The fact that functionals are not H^1-norm equivalent and hence define non-equivalent formulations does not imply that the method is not optimal. It simply means that optimality of the resulting method can not be established a priori using standard elliptic theory.

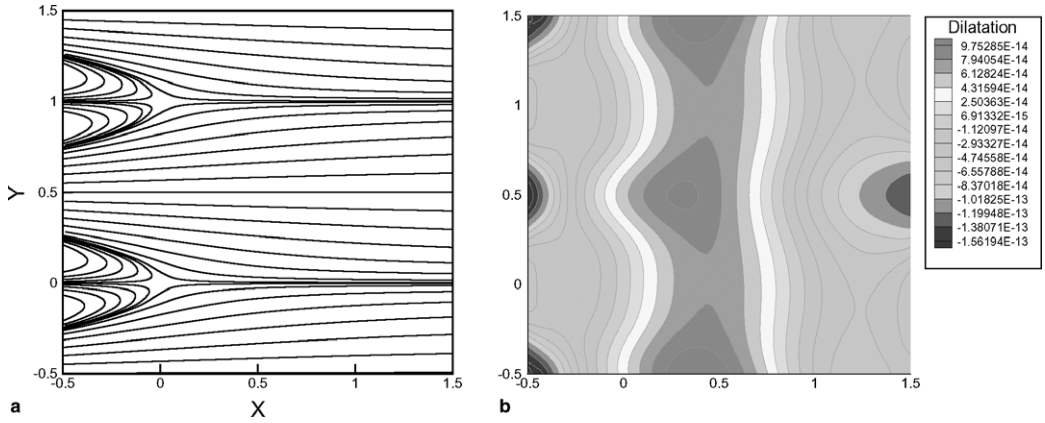

Fig. 1. Kovasznay flow: (a) streamlines for $Re = 40$, (b) dilatation contours for $Re = 40$.

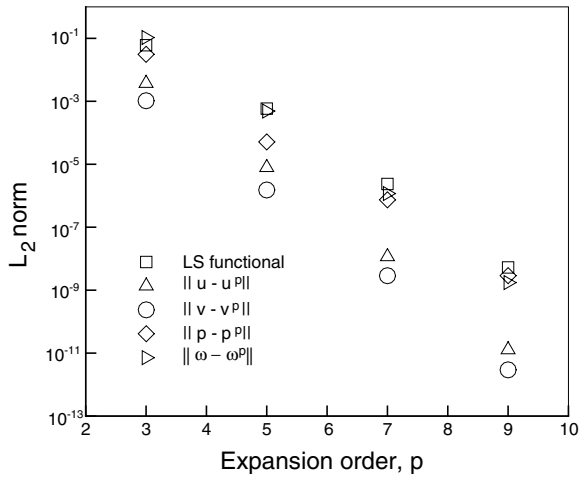

Fig. 2. Convergence of the least-squares functional, velocity, pressure and vorticity fields to the exact Kovasznay solution in the L_2-norm.

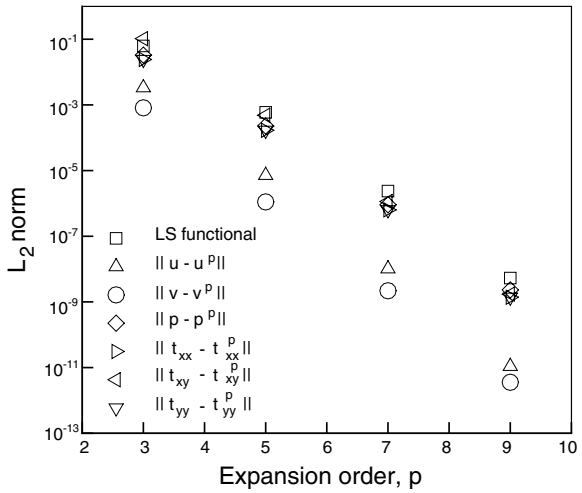

Fig. 3. Convergence of the least-squares functional, velocity, pressure and stress fields to the exact Kovasznay solution in the L_2-norm.

Simulations are carried out for various values of penalty parameters. The p-level used is 9. Newton's iteration does not converge for penalty parameters less than one. For penalty parameter greater than one, non-linear convergence depends on the value of penalty parameter as shown in the following table. Newton's convergence is declared when the relative norm of the residual is less than 10^{-10}. The L_2-norm of least-square functional remains almost the same (5×10^{-9}) and L_2-norm of the residual of continuity equation is below 10^{-12} for all these penalty parameters.

Penalty parameter	No. of Newtons itr.
1	23
5	14
10	13
50	11
100	11

3.2. 2D Lid-driven cavity flow

Next, the two-dimensional lid-driven cavity problem is analyzed to test our formulation. The flow is driven by the translation of the top boundary. No slip boundary condition is imposed on all solid walls. On the top wall ($y = 1.0$) boundary conditions are $u = u(x), v = 0$. To avoid singularity in the boundary condition, we specify a hyperbolic tangent u-velocity distribution on the top wall:

$$u(x) = \begin{cases} \tanh(\beta x), & 0 \leqslant x \leqslant 0.5, \\ -\tanh(\beta(x-1)), & 0.5 < x \leqslant 1.0 \end{cases}$$

with $\beta > 0$. In the present study, $\beta = 100$ and 500 are used, which give a smooth but at the same time sharp transition from $u = 0.0$ to $u = 1.0$ near the walls of the driven surface. This boundary condition results in a well posed boundary condition as singularities at the corners are eliminated. The standard boundary condition ($u = 1$ everywhere) would destroy the high accuracy properties associated with high-order expansions by polluting the solution near the corners. High-order methods are sensitive to these types of singularities. These singularities render the computational method unstable.

We use 18×18 non-uniform mesh which is graded towards the wall; corner elements have the dimension of 0.008×0.008. The eighth-order nodal expansion is used in each element and there are total of 84,100 degrees of freedom in the mesh. All internal degrees of freedom are condensed out, resulting in 20,596 interface

degrees of freedom with a bandwidth of 1148. The banded Cholesky factorization is used to solve for the interface degrees of freedom. In this study, the global nodes are numbered in a natural order and no effort is made to reduce the bandwidth. Bandwidth can be reduced with a suitable choice of a node numbering scheme. An alternate approach to minimize the bandwidth is by using the graph-theory. A popular choice is the reverse Cuthill–McKee permutation [25]. This problem has been solved for the penalty parameter varying from 5 to 40. We use *Re* continuation method and start with $Re = 100$ and march till $Re = 10^4$ at the increment of 300. Results are presented for $\beta = 100$.

Fig. 4(a) contains plots of streamline at $Re = 10^4$. Results match qualitatively very well with the published results of Jiang et al. [12], who used least-squares finite element formulation with an almost uniform 400×408 mesh of bi-linear elements and one-point quadrature. A penalty parameter of 10 is used for these results. The value of the L_2 least-squares functional remains below 1.1×10^{-2} and L_2-norm of the residual of continuity equation is below 3.1×10^{-6} for these computations. Typically it takes two Newton's iterations to converge for every *Re* step. Fig. 4(b) shows pressure contours and Fig. 4(c) contains dilatation contours. Dilatation contours show that mass conservation is satisfied very well locally at all points in the domain with a maximum value of dilatation around 6×10^{-6} near the top corner. Penalty parameter used is only 10 and it works very well for even for this high Reynolds number. This problem is not a very good example to judge required penalty parameter at high *Re*, as there is no mass coming in or going out, problems of flow over a backward-facing step and flow past circular cylinder will test it better.

The *u*-velocity profiles along the vertical mid-line of the cavity $x = 0.5$ are shown in Fig. 5(a) for various values of the penalty parameter and the results are compared with those of Jiang et al. [12]. Again, we see excellent agreement between the two results even for $\gamma = 5$. In Fig. 5(b) *v*-velocity profiles are plotted along the horizontal mid-line of the cavity $y = 0.5$ for various values of the penalty parameter. We note that boundary conditions are

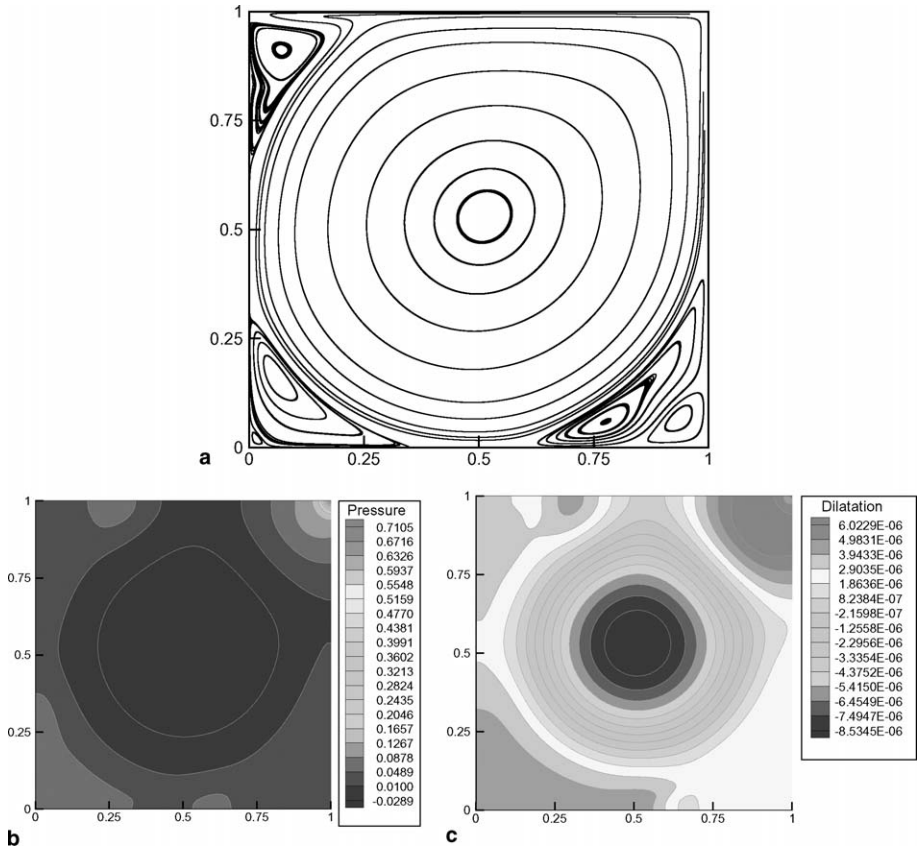

Fig. 4. Numerical results for 2D cavity flow at $Re = 10^4$: (a) streamlines, (b) pressure contours, (c) dilatation contours.

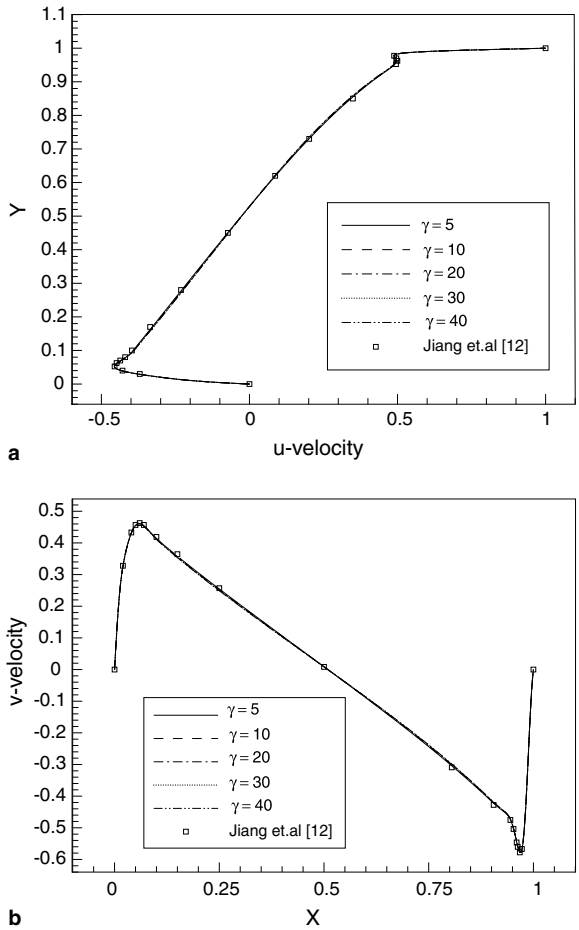

Fig. 5. 2D cavity flow for $Re = 10^4$. (a) Variation of u-velocity with y for various penalty parameters, (b) variation of v-velocity with x for various penalty parameters: comparison with benchmark results.

different for the two studies. Jiang et al. [12] used lid velocity of 1 everywhere while in our case lid velocity varies with x as shown in Fig. 7 ($\beta = 100$).

Next, PCG convergence history is plotted for four Newton's iterations for $Re = 100$ in Fig. 6. We use 10×10 grid with the corner element having dimension of 0.05×0.05. The p-level used is 7 and the penalty parameter is taken to be 10. Zero initial guess is used for all variables including pressure. There are no pronounced fluctuations.

As Figs. 5(a) and (b) show, formulation gives very accurate results for even penalty parameter of 5. Typical penalty parameter values used in the traditional penalty finite element formulation are in the range of 10^8–10^{12}. For such a high penalty parameter, conditioning number of the resulting coefficient matrix becomes very high and different order integration rule is used to integrate penalty terms to obtain *acceptable* solution. Some explanations have been given in the literature to justify the use of different order integration schemes for various terms of the coefficient matrix. In this study, we have used equal order integration for all terms.

We solve this problem for $\beta = 500$ also on two different grids 18×18 and 22×22 with corner element having dimension 0.008×0.008 and 0.007×0.007, respectively, with eighth-order nodal expansion in each element ($\gamma = 20$). Variation of lid velocity with x for $\beta = 100$ and 500 is shown in Fig. 7. They closely emulate the standard ill-posed boundary condition. Fig. 8 shows that on 18×18 mesh results are not satisfactory while results are accurate on 22×22 mesh. We see that even for singular boundary conditions (close to 1) accurate results can be obtained with h-refinement. For singular boundary conditions simulation becomes unstable (Newton's iterations do not converge) around Reynolds number of 7100 for 18×18 mesh. The Reynolds number at which the simulation becomes unstable depends on the h-refinement used.

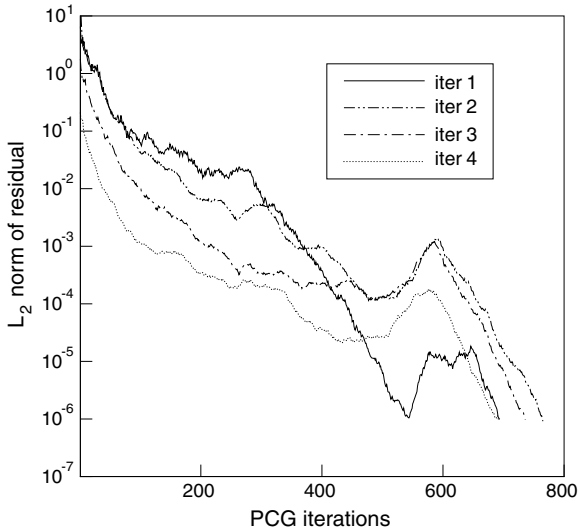

Fig. 6. Convergence history of preconditioned conjugate gradient solver (PCG) for 2D cavity flow.

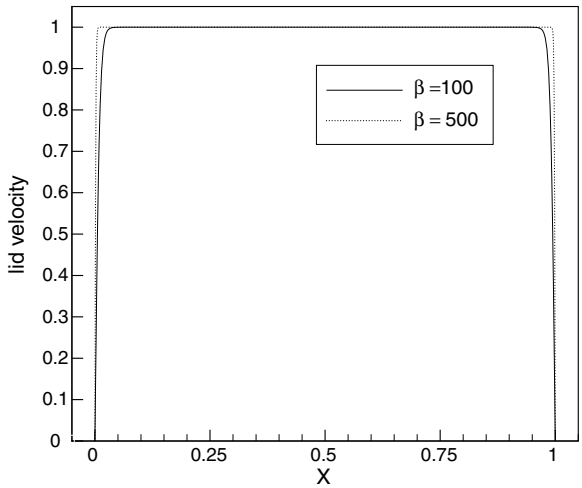

Fig. 7. Variation of lid velocity with parameter β.

3.3. Flow over a backward-facing step

Next, we consider two-dimensional steady flow over a backward-facing step at $Re = 800$. The geometry and boundary conditions, taken from the benchmark solution of Gartling [13], are shown in Fig. 9. No-slip boundary condition is imposed on all walls. Boundary condition of $u(y) = 0$ is imposed for $-0.5 \leqslant y \leqslant 0.0$. A parabolic velocity profile given by $u(y) = 24y(0.5 - y)$ is specified at the inlet for $0.0 \leqslant y \leqslant 0.5$. This produces a maximum inflow velocity of $u_{\max} = 1.5$ and a mean inflow velocity of $u_{\text{avg}} = 1.0$. The Reynolds number is based on the mean inflow velocity. At the outflow, boundary condition is implemented as described earlier in Section 2.3. The domain, $\bar{\Omega} = [0, 30] \times [-0.5, 0.5]$, is discretized using 32 elements as shown in Fig. 9. To accurately resolve primary and secondary circulation zones, a non-uniform mesh is used. Interface nodes are shown with squares while interior nodes are shown with triangles. We use 11th-order nodal expansion in each element. There are 16,284 degrees of freedom in the mesh. We condense out all interior degrees of freedom, resulting in 3434 interface degrees of freedom and a bandwidth of 260. In this case, the nodes are numbered in the y-direction first to reduce the bandwidth. One might think to use a very high p-level to reduce interface degrees of freedom and bandwidth (which will also reduce memory storage) but in that case cost of

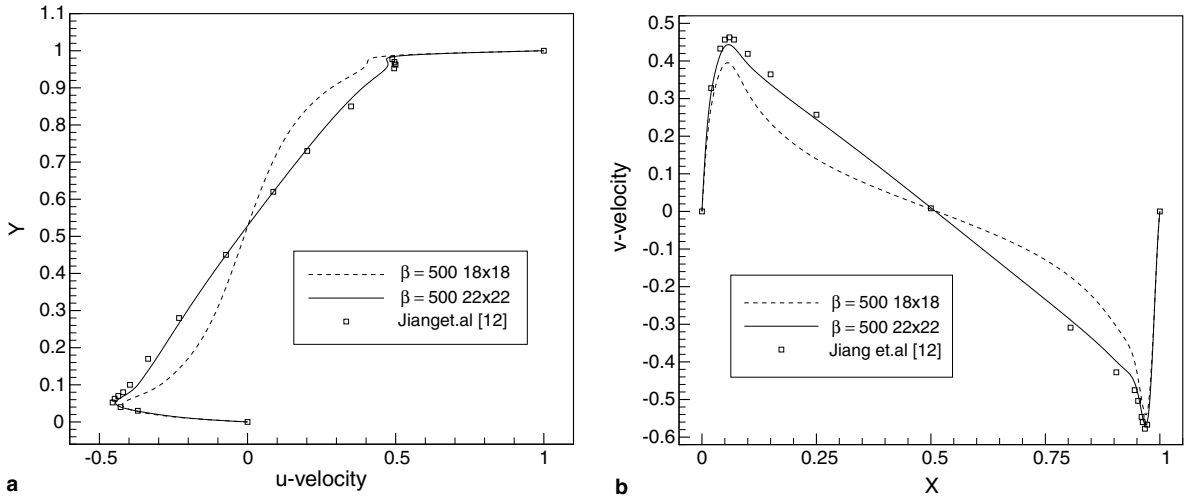

Fig. 8. (a) Variation of u-velocity with y for two different meshes, (b) variation of v-velocity with x for two different meshes.

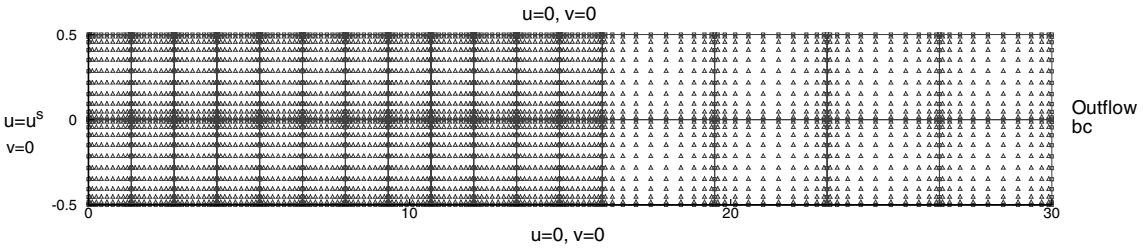

Fig. 9. Mesh and boundary conditions for flow over a backward-facing step.

elemental matrix inversion will be high to construct the Schur complement. Simulations are carried out for penalty parameter of 5–30. We use Re continuation method and start with $Re = 100$ and march till $Re = 800$ with an increment of 100.

Fig. 10 contains plots of streamlines, pressure and dilatation contours for the penalty parameter of 20. Results match qualitatively very well with the published results of Pontaza and Reddy [1]. After reattachment of the upper wall eddy, the flow slowly recovers towards a fully developed Poiseuille flow. Flow is almost fully developed at the exit ($x = 30$) with no pressure gradient in y direction. This is because outlet boundary condition of $p = 0$ also gives good results. The value of the L_2 least-squares functional remains below 3×10^{-2} and L_2-norm of the residual of continuity equation is below 1.1×10^{-5} for these computations. Fig. 10(c) shows dilatation contours, which are similar to the pressure contours. Dilatation has a high value in the reattachment zone where there are sharp gradients.

The u-velocity profiles along the channel height at $x = 7$ and $x = 15$ are compared with the benchmark results of Gartling [13] in Fig. 11 for penalty parameter of 20. We find excellent agreement. Pressure profiles along the length of the channel are plotted in Fig. 12 for penalty parameters of 5, 10, 20 and 30 and compared with the result of Pontaza and Reddy [1]. They give identically same results and match well with that of [1]. A comparison of primary reattachment length (S_1), secondary separation length (S_2), and secondary reattachment length (S_3) for various values of penalty parameter is presented in the following table. Accurate values of reattachment lengths are found by running stress based formulation where stresses are primary variables.

	$\gamma = 5$	$\gamma = 10$	$\gamma = 20$	$\gamma = 30$	Gartling [13]
S_1	6.17	6.11	6.10	6.10	6.10
S_2	4.93	4.87	4.86	4.85	4.85
S_3	10.43	10.47	10.48	10.48	10.48

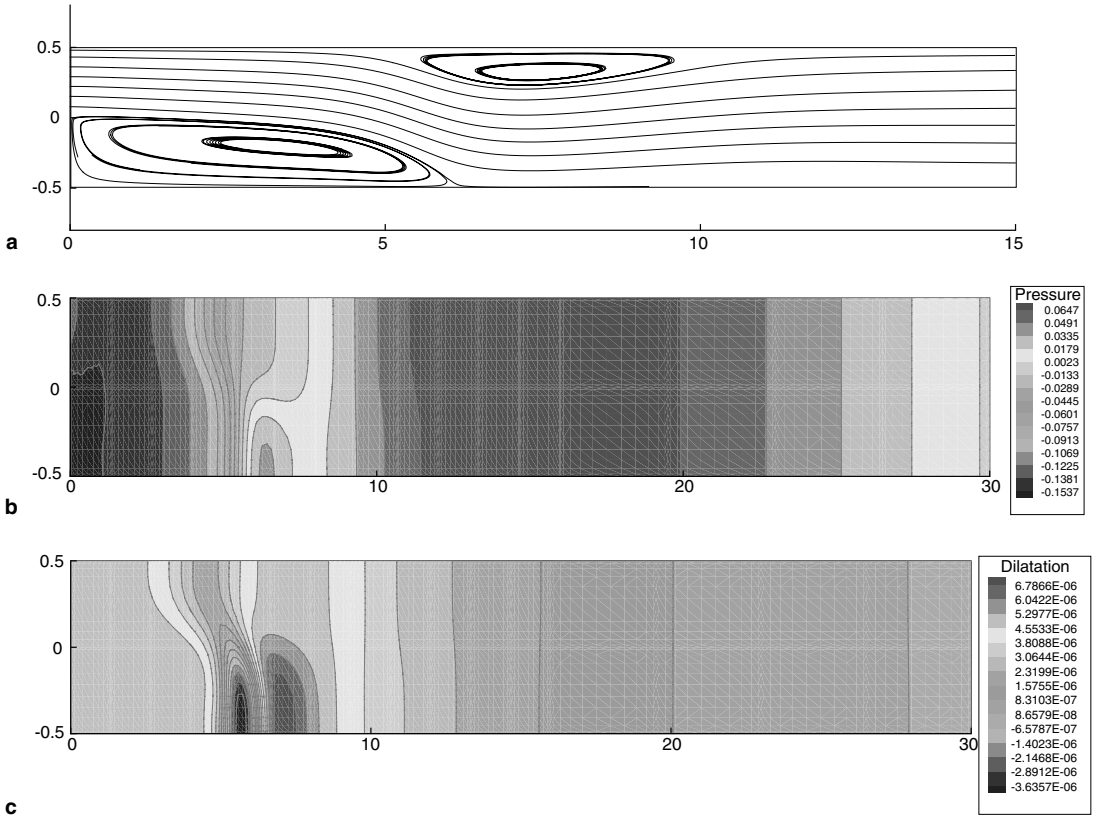

Fig. 10. Flow over a backward-facing step at $Re = 800$: (a) streamlines, (b) pressure contours, (c) dilatation contours.

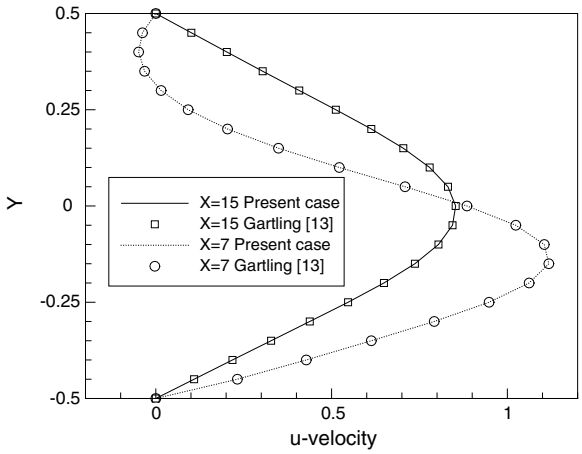

Fig. 11. Flow over a backward-facing step at $Re = 800$: horizontal velocity profiles along the height of the channel.

Next, PCG convergence history is plotted (see Fig. 13). We present this formulation as an alternative to *hp* least-square formulation of Pontaza and Reddy [1,2]. To compare PCG history, we run the simulation on 10×2 uniform grid and use 11th-order polynomial expansion (same as used in [1]). They reported that for $Re = 800$ with solution of $Re = 700$ as initial guess, it takes four Newton's iterations to converge and it takes approximately 4500, 3500, 2500 and 700 PCG iterations to converge when the Jacobi preconditioner is used. In our case for penalty parameter of 40, it takes six Newton's iterations to converge and it takes approximately

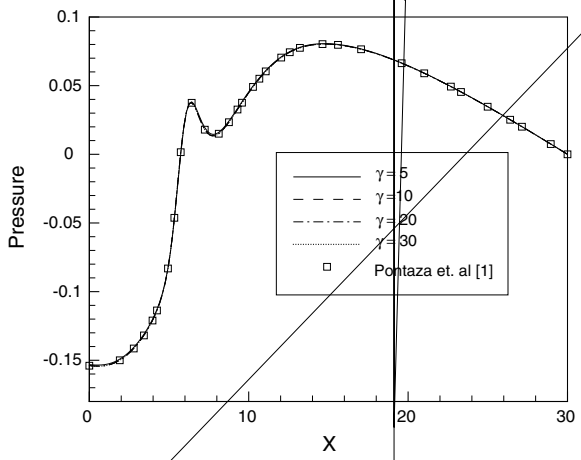

Fig. 12. Variation of lower wall pressure with horizontal position for different values of penalty parameter: comparison with Pontaza and Reddy [1].

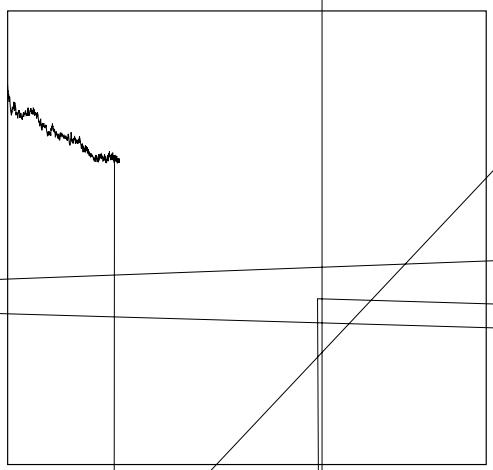

1850, 1600, 1850, 1850, 1800 and 1500 iterations to converge; PCG convergence is declared when L_2-norm of residual is below 10^{-6} in both the cases. The only difference is that Pontaza and Reddy did not use Schur complement method. Another small difference is that they used modal basis but modal basis has, in general, slightly better conditioning than the nodal basis. Both formulations have the same number of independent variables (4). Its clear from this plot that conditioning of coefficient matrix is almost the same as that produced by *hp* least-squares formulation of Pontaza and Reddy [1].

3.4. Flow past a circular cylinder at low Reynolds number

The third benchmark problem considered here is the steady two-dimensional flow of an incompressible fluid past a circular cylinder. The Reynolds number is taken to be 40, for which a steady-state solution exists. Domain of interest is $[-10.0, 15.0] \times [-10.0, 10.0]$. The x-component of inlet velocity (u) is specified to be 1.0 and the y-component (v) is set to zero. Symmetry boundary conditions, $\omega = 0$ and $v = 0$, are imposed on the top and bottom walls. The outflow boundary conditions are imposed in a weak sense through the least-squares functional.

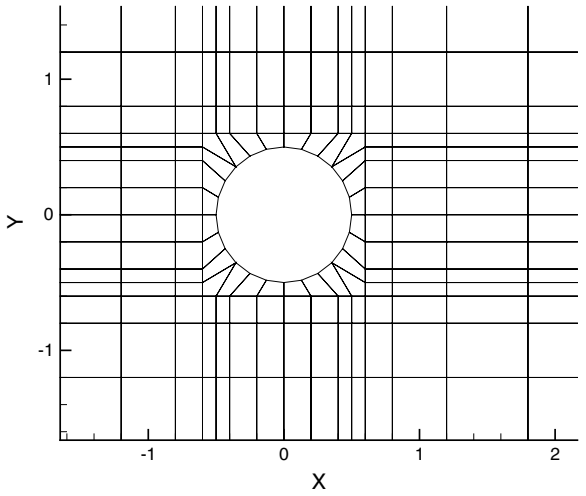

Fig. 14. Close-up view of the geometric discretization around the cylinder.

Fig. 14 contains a close-up view of the geometric discretization around the circular cylinder. We generate orthogonal mesh using rectangular elements everywhere in the domain except around the cylinder. One layer of body fitting mesh is generated around the cylinder. At this point we will digress a bit and talk about reducing computational cost for high-order finite element based formulations. For rectangular elements Jacobian matrix is of the form (see [16,17])

$$J = \begin{pmatrix} \frac{h_1}{2} & 0 \\ 0 & \frac{h_2}{2} \end{pmatrix}$$

and global derivatives of shape functions are

$$\begin{pmatrix} \frac{\partial \psi_i^e}{\partial x} \\ \frac{\partial \psi_i^e}{\partial y} \end{pmatrix} = J^{-1} \begin{pmatrix} \frac{\partial \psi_i^e}{\partial \xi} \\ \frac{\partial \psi_i^e}{\partial \eta} \end{pmatrix} = \begin{pmatrix} \frac{2}{h_1} \frac{\partial \psi_i^e}{\partial \xi} \\ \frac{2}{h_2} \frac{\partial \psi_i^e}{\partial \eta} \end{pmatrix},$$

where $\frac{\partial \psi_i^e}{\partial \xi}$ and $\frac{\partial \psi_i^e}{\partial \eta}$ are local derivatives of shape functions. Therefore, calculation of global derivatives of the shape functions is straightforward. In the case of curved elements, we need to calculate Jacobian matrix for each element and carry out matrix multiplications to obtain global derivatives of the shape functions, which is computationally costly (see [16]). Such grids reduce a lot of computational time. It is to be mentioned that even for moderate size problems we cannot store global derivatives of shape functions for all elements of the mesh. In order to accurately represent the curved boundary, we implement an isoparametric formulation; i.e., we use the same expansion order to interpolate dependent variables and the geometry.

We use two-dimensional incompressible Navier–Stokes equations in the dilatation–vorticity first-order form. There are 424 quadrilateral elements in the mesh. The seventh-order nodal expansions are used in each element. Discrete model contains 84,644 degrees of freedom. We condense out all interior degrees of freedom. There are 23,588 interface degrees of freedom and bandwidth of the system is 1256.

Fig. 15 contains plots of streamlines and pressure contours and dilatation contours for $\mathrm{Re} = 40$ and $\gamma = 20$. The value of the recirculation length is found to be 4.55 cylinder radius. Our result is in good agreement with the numerical value of 4.50 cylinder radius by Kawaguti and Jain [26], whereas Dennis and Chang [27] reported a recirculation length of 4.69 cylinder radius. The value of the L_2 least-squares functional remains below 1.3×10^{-2}.

A comparison of the experimental values of the surface pressure coefficient distribution along the cylinder surface with the computed values is shown in Fig. 16 for the penalty parameters of 20, 30, and 40. Experimental values are taken from Grove et al. [14]. Our results are in good agreement with the experimental measurements. Pressure coefficient distribution is almost same for the all the penalty parameters considered here. Drag coefficient is $C_D = 1.55$ which is in good agreement with the published results of Tritton [28], who reported it to be 1.56.

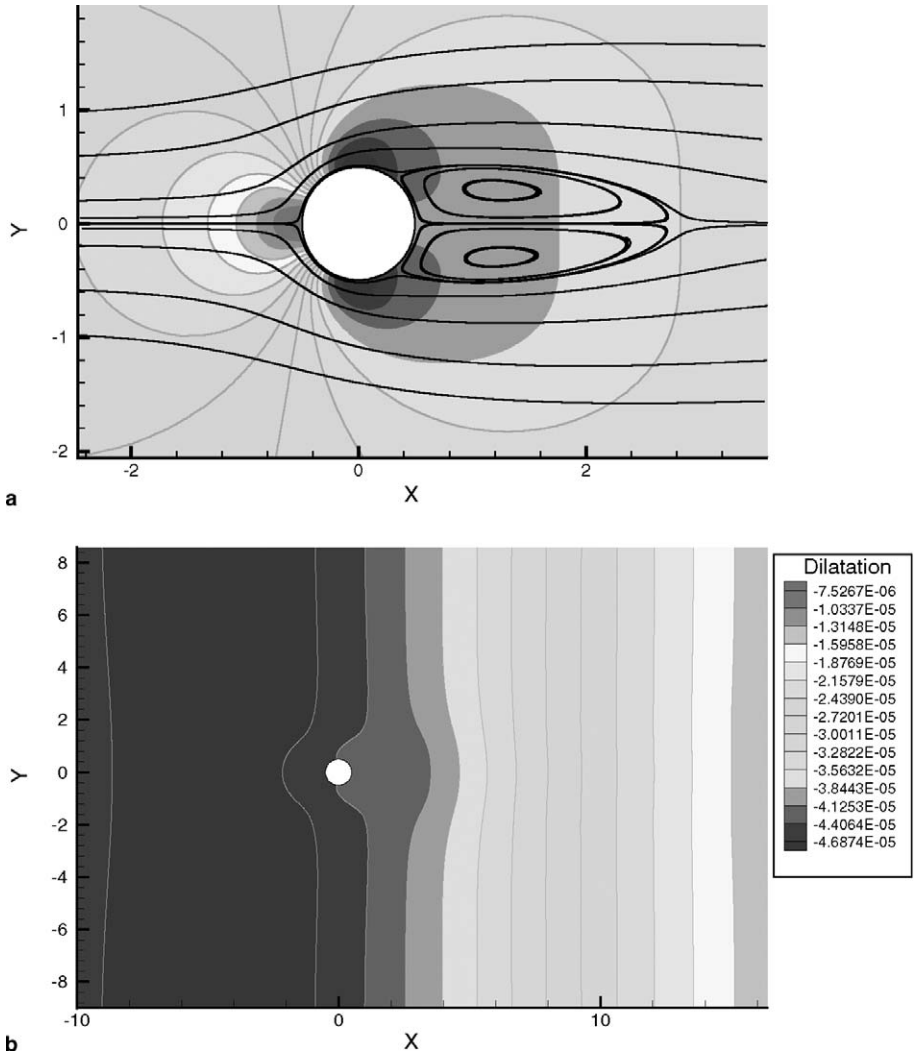

Fig. 15. Flow past a circular cylinder at $Re = 40$: (a) streamlines and pressure contours, (b) dilatation contours.

It has been seen earlier that non-linear convergence is dependent on penalty parameter. For very low value of penalty parameter (1–10) Newton's convergence is slow (this value is problem dependent). In Fig. 17(a) non-linear convergence is plotted for various values of penalty parameter. The plot reveals that convergence is slow for $\gamma = 20$. In Fig. 17(b) we plot pressure convergence history. For all the problem solved in this paper pressure convergence is almost the same as the non-linear convergence but one needs to make sure that pressure also converges. For very low value of the penalty parameter, pressure convergence is slow, which in turn slows non-linear convergence.

3.5. Flow past a large circular cylinder in a channel

We tested this formulation for various problems but they do not test mass conservation rigorously. To test mass conservation rigorously, we solve flow past a large circular cylinder in a channel with blockage ratio of 2 ($H/D = 2$). Chang and Nelson [29] used similar problem to test mass conservation for Stokes flow. Domain of interest is $[-5.0, 10.0] \times [-1.0, 1.0]$. Cylinder has unit diameter and it is centered at $(0.0, 0.0)$. We use similar grid as used earlier for flow past a circular cylinder. A p-level of 6 is used and there are 76,584 degrees of freedom in the mesh. Mesh is fine near the cylinder. No-slip boundary conditions are imposed on side walls. At inlet boundary

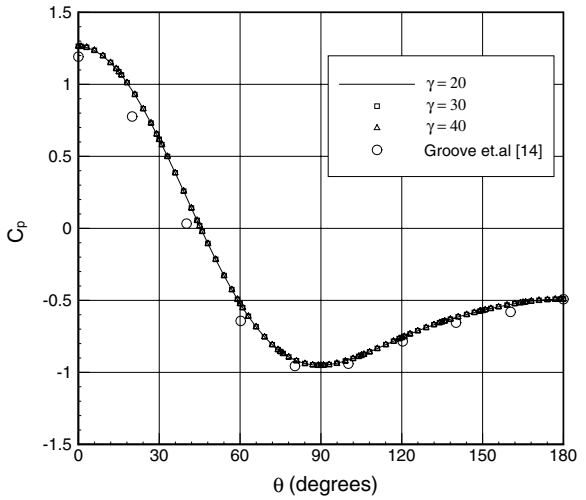

Fig. 16. Pressure coefficient distribution along the cylinder surface for various values of penalty parameter.

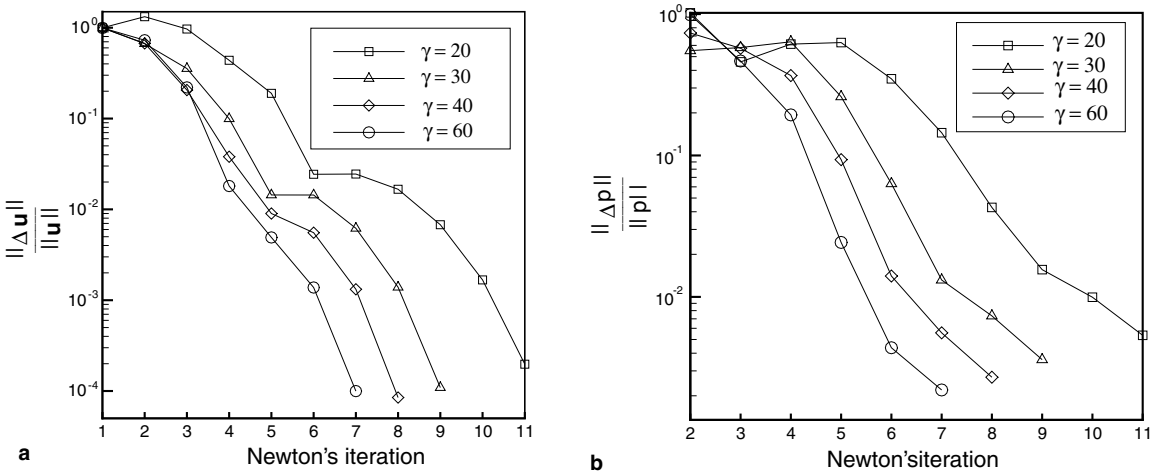

Fig. 17. (a) Non-linear convergence for various values of penalty parameter, (b) pressure convergence for various values of penalty parameter.

conditions are $u = 1.0$ and $v = 0.0$. The outflow boundary conditions are imposed in a weak sense through the least-squares functional. Reynolds number considered here is 40 for which steady state solution exists.

Fig. 18(a) shows streamline plot. In this case separation is delayed. u-Velocity contours around the cylinder are shown in Fig. 18(b). We calculate mass flow rate at the inlet, outlet and section $x = 0$ and we find very good mass conservation as shown by the following table. We solved this problem using *hp* least-squares formulation [1] also (under same conditions) and calculated mass flow rates. Even for low values of penalty parameter, present formulation conserves mass better than *hp* least-squares formulation [1] does.

	$\gamma = 40$	$\gamma = 70$	*hp* Least-squares
Inlet	2.000	2.000	2.000
$x = 0$	1.982	1.986	1.974
Outlet	1.987	1.991	1.975

In Fig. 19 we plot dilatation contours for the penalty parameter of 40. Mass conservation is satisfied to a very good extent as shown by this plot. It requires a bit higher value of penalty parameter compared to the last

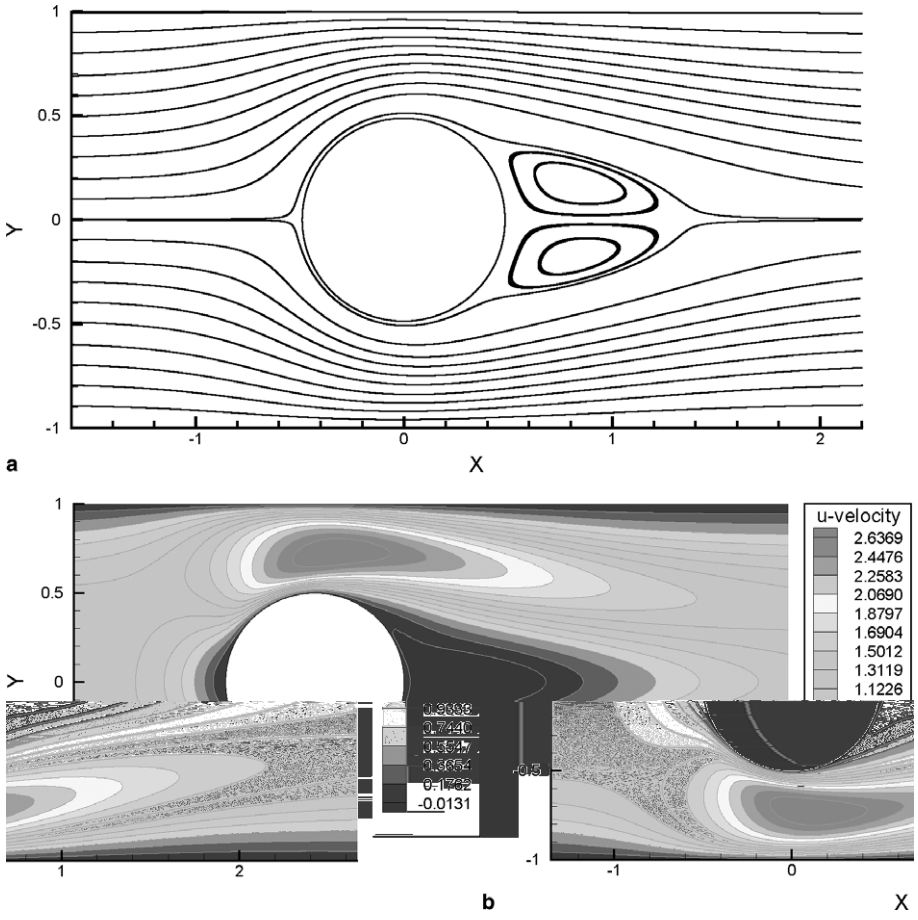

Fig. 18. Flow past a large circular cylinder in a channel: (a) streamlines, (b) u-velocity contours.

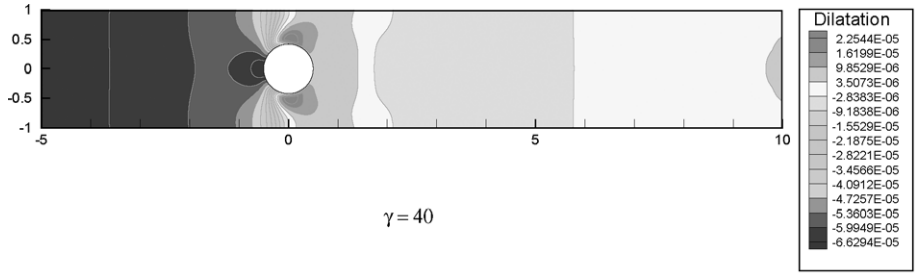

Fig. 19. Dilatation contours for flow past a large circular cylinder.

example. Dilatation values are a bit high at the inlet. This might be because we use very coarse grid at the inlet. This example shows that even for very low values of the penalty parameter, mass conservation is satisfied to a very good extent in this formulation.

4. Temperature–velocity coupled problem

Here, we consider steady incompressible fluid flow in a domain $\Omega \subset \mathbb{R}^2$ bounded by $\Gamma = \Gamma_\theta \cup \Gamma_q$, where Γ_θ and Γ_q are the isothermal and the adiabatic boundaries as well as $\Gamma_\theta \cap \Gamma_q = \emptyset$. The fluid motion is induced by

the temperature gradient across the vertical walls. The buoyancy effect is approximated by the Boussinesq assumption. The Navier–Stokes equations and the energy equation in dimensionless form are given below.

Find the velocity $\mathbf{u}(\mathbf{x})$, pressure $p(\mathbf{x})$ and temperature $\theta(\mathbf{x})$ such that

$$(\mathbf{u}\cdot\nabla)\mathbf{u}+\nabla p-\frac{1}{Re}\nabla\cdot\left[(\nabla\mathbf{u})+(\nabla\mathbf{u})^{\mathrm{T}}\right]+\theta\frac{\mathbf{g}}{|\mathbf{g}|}=\mathbf{0}\quad\text{in }\Omega, \tag{31}$$

$$\nabla\cdot\mathbf{u}=0\quad\text{in }\Omega, \tag{32}$$

$$(\mathbf{u}\cdot\nabla)\theta-\frac{1}{Pe}\nabla^{\mathbf{2}}\theta=0\quad\text{in }\Omega, \tag{33}$$

$$\mathbf{u}=\mathbf{u}^{s}\quad\text{on }\Gamma_{u}, \tag{34}$$

$$\hat{\mathbf{n}}\cdot\boldsymbol{\sigma}=\mathbf{f}^{s}\quad\text{on }\Gamma_{f}, \tag{35}$$

$$\theta=\theta^{s}\quad\text{on }\Gamma_{\theta}, \tag{36}$$

$$\hat{\mathbf{n}}\cdot\mathbf{q}=q^{s}\quad\text{on }\Gamma_{q}, \tag{37}$$

where $\mathbf{g}$ is gravitational acceleration vector which is acting in negative y-direction. Here we take the cavity wall length and buoyant speed $((|\mathbf{g}|\alpha\Delta\theta l)^{1/2})$ as characteristic length and velocity, respectively. The characteristic numbers are $Re=(Ra/Pr)^{1/2}$, $Pe=(Ra\,Pr)^{1/2}$, $Ra=\alpha|g|l^{3}\Delta\theta/(\kappa\nu)$ and $Pr=\nu/\kappa$, where α is the volumetric thermal expansion coefficient, l is the characteristic length, $\Delta\theta$ is the characteristic temperature, κ is the thermal diffusivity, and $\nu=\mu/\rho$ is the kinematic viscosity.

4.1. The vorticity–dilatation/heat flux based first-order system

To make the system first-order, we introduce vorticity–dilatation and heat flux vector as independent variables. The resulting first-order system in dimensionless form can be stated as follows:

Find the velocity $\mathbf{u}(\mathbf{x})$, dilatation $D(\mathbf{x})$, vorticity $\boldsymbol{\omega}(\mathbf{x})$, temperature $\theta(\mathbf{x})$ and heat flux $\mathbf{q}(\mathbf{x})$ such that

$$(\mathbf{u}\cdot\nabla)\mathbf{u}-\gamma\nabla D+\frac{1}{Re}\nabla\times\boldsymbol{\omega}+\theta\frac{\mathbf{g}}{|\mathbf{g}|}+\nabla p^{n-1}=\mathbf{0}\quad\text{in }\Omega, \tag{38}$$

$$\boldsymbol{\omega}-\nabla\times\mathbf{u}=\mathbf{0}\quad\text{in }\Omega, \tag{39}$$

$$D-\nabla\cdot\mathbf{u}=0\quad\text{in }\Omega, \tag{40}$$

$$(\mathbf{u}\cdot\nabla)\theta+\nabla\cdot\mathbf{q}=0\quad\text{in }\Omega, \tag{41}$$

$$\mathbf{q}+\frac{1}{Pe}\nabla\theta=\mathbf{0}\quad\text{in }\Omega, \tag{42}$$

$$\mathbf{u}=\mathbf{u}^{s}\quad\text{on }\Gamma_{u}, \tag{43}$$

$$\boldsymbol{\omega}=\boldsymbol{\omega}^{s}\quad\text{on }\Gamma_{\omega}, \tag{44}$$

$$\theta=\theta^{s}\quad\text{on }\Gamma_{\theta}, \tag{45}$$

$$\hat{\mathbf{n}}\cdot\mathbf{q}=q^{s}\quad\text{on }\Gamma_{q}. \tag{46}$$

The L_2 least-squares formulation and finite element model development proceed in a similar manner as described for the incompressible Navier–Stokes equations.

4.2. Numerical example: buoyancy-driven flow inside a square enclosure

As a numerical example, we consider two-dimensional, steady, buoyancy-driven flow in a square enclosure with differentially heated vertical walls. The square enclosure is taken to be the unit square, $\bar{\Omega}=[0,1]\times[0,1]$. A finite element mesh of 10×10 non-uniform quadrilateral finite elements is used to discretize the domain with the corner element having dimension 0.02×0.02. No slip velocity boundary condition is imposed on all solid walls. q_y is 0 at the top and bottom walls while left side wall is kept at $\theta=1$ and right side wall at $\theta=0$.

Computations have been performed for Rayleigh numbers of 10^4, 10^5, 10^6. Air is taken as the working fluid with Prandtl number 0.71; seventh-order nodal expansion is used. There are seven degrees of freedom at each

node. There are total 35,287 degrees of freedom in the mesh. We condense out all interior degrees of freedom. There are 10,087 interface degrees of freedom and bandwidth of the system is 1015. The discrete model is linearized using Newton's method and algebraic equations are solved using the banded Cholesky factorization. Computations have been performed for penalty parameters of 10, 20, and 30.

The Nusselt number on the vertical boundary at $x = 0$ is calculated as

$$Nu(y) = q_x(y)\,Pe$$

and the average Nusselt number (at $x = 0$) is calculated as

$$\overline{Nu} = \int_0^1 Nu(y)\,\mathrm{d}y.$$

Components of heat flux are taken to be the primary variables. Therefore, in spite of using C^0 continuous basis functions, we obtain smooth solution for heat fluxes. The average Nusselt number on the boundary is calculated using numerical integration using 8-point Gauss quadrature. We use *Ra* continuation method, start with $Ra = 10^5$ and proceed till 10^6 with *Ra* increment of 10^5. Zero initial guess is used for $Ra = 10^5$. It takes 10

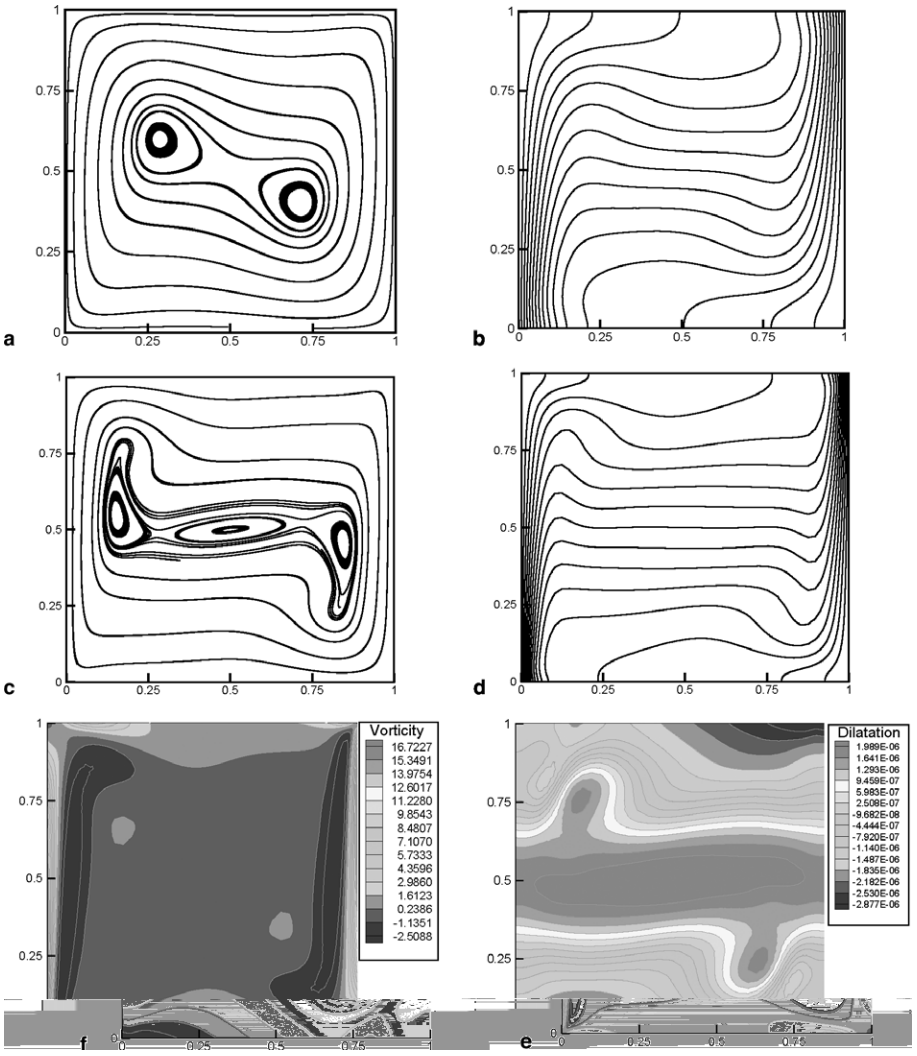

Fig. 20. Numerical results for 2D thermal cavity flow: (a) streamlines at $Ra = 10^5$, (b) temperature contours for $Ra = 10^5$, (c) streamlines for $Ra = 10^6$, (d) temperature contours for $Ra = 10^6$, (e) vorticity contours for $Ra = 10^6$, (f) dilatation contours for $Ra = 10^6$.

Newton's iterations to converge for $Ra = 10^5$. Subsequent Rayleigh numbers take 2–3 Newton's iterations to converge. The value of the L_2 least-squares functional remains below 1×10^{-4} for all Rayleigh numbers.

Fig. 20 contains plots of streamlines of the flow field and temperature distribution for Rayleigh numbers of 10^5 and 10^6. The patterns exhibit the required centrosymmetry and are in qualitative agreement with previously reported numerical results of Davis [15]. Fig. 20(e) shows vorticity contours which match well qualitatively with that of [15]. In Fig. 20(f) dilatation contours are plotted. Mass conservation is satisfied to very good extent. Maximum dilatation value is of the order 10^{-6}. Fig. 21(a) contains the plot of u-velocity profile along the vertical mid-line for penalty parameters of 10, 20 and 30. All three penalty parameters give identical values. Fig. 21(b) contains plots of temperature distributions along the vertical mid-line for three penalty parameters. Although the penalty parameter does not appear directly in the energy equation, there will be an effect of it on the temperature field since the temperature field depends on the velocity field for both coupled and decoupled formulations. Again all three penalty parameters give identical values. The average Nusselt number on the vertical boundary of the cavity at $x = 0$ for three Rayliegh numbers are compared with the benchmark result of Davis [15] in the following table:

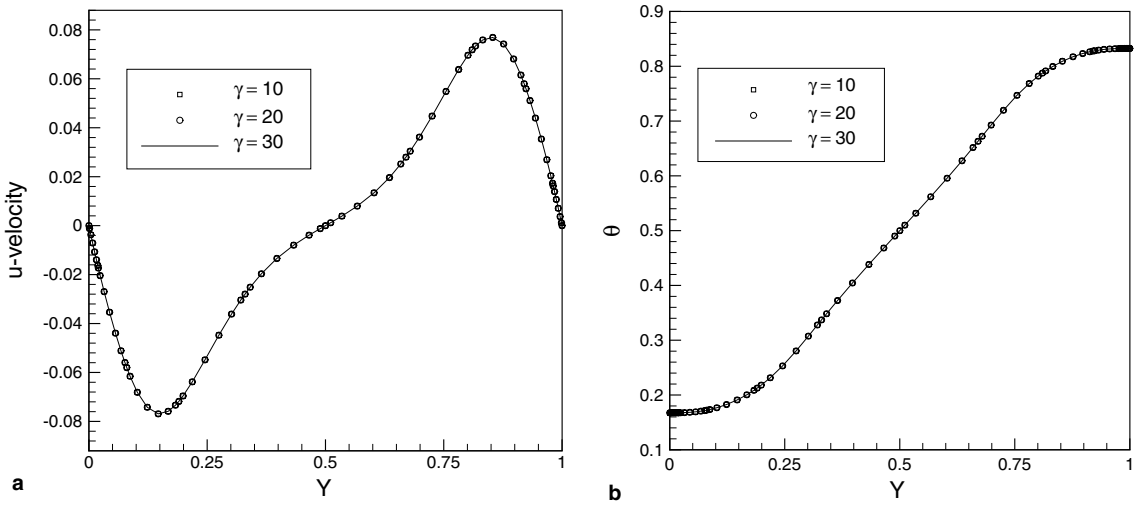

Fig. 21. (a) u-Velocity, (b) temperature along the vertical mid-line of the enclosure $Ra = 10^6$.

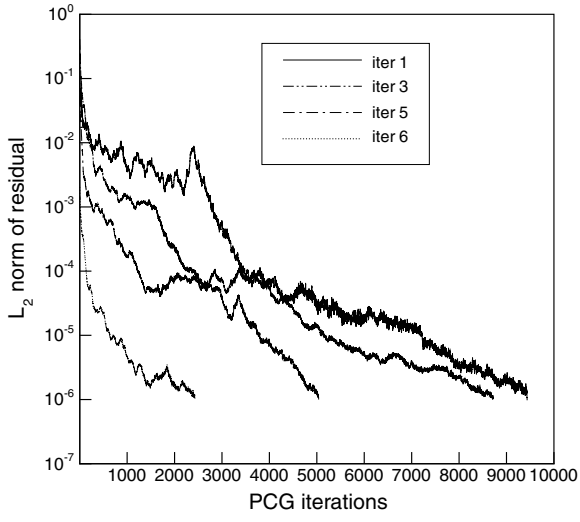

Fig. 22. Convergence history of preconditioned conjugate gradient solver (PCG) for thermal cavity problem.

	$\gamma = 5$	$\gamma = 10$	$\gamma = 20$	Davis [15]
$Ra = 10^4$	2.244	2.244	2.244	2.238
$Ra = 10^5$	4.521	4.522	4.522	4.509
$Ra = 10^6$	8.824	8.824	8.825	8.817

In Fig. 22 we plot PCG convergence history for $Ra = 10^4$. Zero initial guess is used. It takes six Newton's iterations to converge. Penalty parameter is 10. Again PCG converges steadily without much fluctuation.

5. Concluding remarks

In this paper, we presented spectral/hp penalty least-squares finite element formulation for the steady incompressible Navier–Stokes equations and its validation and applications to a variety of benchmark problems. Continuity equation was treated as a constraint on velocity field and this constraint was imposed using the penalty method, eliminating pressure from the model. Spectral convergence of the L_2 least-squares functional was verified using the Kovasznay flow solution to the incompressible Navier–Stokes equations. Both vorticity–dilatation and stress based first-order systems achieved spectral convergence for all the variables including pressure. Numerical results for incompressible 2D lid-driven cavity flow, flow over a backward-facing step, steady flow past a circular cylinder, flow past a large circular cylinder in a channel, and buoyant flow inside a square enclosure were presented. In all cases, the present results were found to be in excellent agreement with benchmark solutions available in the literature. For all numerical examples, the effect of penalty parameter on the accuracy was investigated thoroughly and it was concluded that the present model gives very accurate results even for low penalty parameters (10–40).

We presented this formulation as an alternative of spectral/*hp* least-squares finite element formulation of Pontaza and Reddy [1,2], where the continuity residual is retained in the least-squares functional and enforced in a least-squares sense. In the present formulation, the incompressibility condition can be satisfied to any extent by a suitable value for the penalty parameter. Present formulation carries equal number of independent variables as spectral/*hp* least-squares [1] carries. We presented PCG convergence history of all the problems solved and plots show that coefficient matrix is well conditioned. We compared PCG history with that of spectral/*hp* least-squares [1] and found similar convergence.

The present penalty least-squares finite element model is a better alternative to traditional weak form penalty finite element model also. Advantage of the present model is that it gives very accurate results for very low penalty parameters. In addition, there is no need to under-integrate penalty terms of the coefficient matrix. We have computed pressure for all the problems solved herein and compared with benchmarks results whenever available. We note that the computed pressure fields are continuous in this formulation as opposed to weak form penalty finite element formulation, and their values are found to be in excellent agreement with published results. This penalty least-squares formulation produces a symmetric positive-definite coefficient matrix while the weak form penalty finite element formulation produces non-symmetric coefficient matrix.

Acknowledgments

The authors gratefully acknowledge the support of this work by the Computational Mathematics Program of the Air Force Office of Scientific Research through Grant F49620-03-1-0201 and Structural Dynamics Program of Army Research Office through Grant 45508-EG. The authors are pleased to acknowledge the constructive comments on the manuscript by Dr. J.P. Pontaza.

References

[1] J.P. Pontaza, J.N. Reddy, Spectral/*hp* least-squares finite element formulation for the Navier–Stokes equations, J. Comput. Phys. 190 (2003) 523.

[2] J.P. Pontaza, J.N. Reddy, Space–time coupled spectral/*hp* least-squares finite element formulation for the incompressible Navier–Stokes equations, J. Comput. Phys. 197 (2004) 418.

[3] I. Babuska, Errors bounds for finite element method, Numer. Math. 16 (1971) 322.
[4] F. Brezzi, K.J. Bathe, A discourse on the stability conditions for mixed finite element formulations, Comput. Meth. Appl. Mech. Eng. 82 (1990) 27.
[5] O.C. Zienkiewicz, Constrained variational principles and penalty function methods in finite element analysis, in: Lecture Notes in Mathematics: Conference on the Numerical Solution of Differential Equations, 1974, p. 207.
[6] D.S. Malkus, T.J.R. Hughes, Mixed finite element methods – reduced and selective integration techniques: a unification of concepts, Comput. Meth. Appl. Mech. Eng. 15 (1978) 63.
[7] T.J.R. Hughes, W.K. Liu, Finite element analysis of incompressible viscous flows by the penalty function formulation, J. Comput. Phys. 30 (1979) 1.
[8] P. Bochov, M.D. Gunzburger, Least-squares finite-element methods for optimization and control problems for the Stokes equations, Comput. Math. Appl. 48 (2004) 1035.
[9] J.S. Hesthaven, Spectral penalty methods, Appl. Numer. Math. 33 (2000) 23.
[10] P.J. Diamessis, J.A. Domaradzki, J.S. Hesthaven, A spectral multidomain penalty method model for the simulation of high Reynolds number localized incompressible stratified turbulence, J. Comput. Phys. 202 (2005) 298.
[11] M.D. Gunzburger, Iterated penalty methods for the Stokes and Navier–Stokes equations, in: T.J. Chung, G.R. Karr (Eds.), Finite Element Analysis in Fluids, Proceedings of the 7th International Conference on Finite Element Methods in Flow Problems, University of Alabama Press, 1989, p. 1040.
[12] B.N. Jiang, T.L. Lin, L.A. Povinelli, Large-scale computation of incompressible viscous flow by least-squares finite element method, Comput. Meth. Appl. Mech. Eng. 114 (1994) 213.
[13] D.K. Gartling, A test problem for outflow boundary conditions – flow over a backward-facing step, Int. J. Numer. Meth. Fluids 11 (1990) 953.
[14] A.S. Grove, F.H. Shair, E.E. Petersen, A. Acrivos, An experimental investigation of the steady separated flow past a circular cylinder, J. Fluid Mech. 19 (1964) 60.
[15] G.D.V. Davis, Natural convection of air in a square cavity: a bench mark numerical solution, Int. J. Numer. Meth. Fluids. 3 (1983) 249.
[16] J.N. Reddy, An Introduction to the Finite Element Method, third ed., McGraw-Hill, New York, 2006.
[17] J.N. Reddy, Introduction to Nonlinear Finite Element Analysis, Oxford University Press, Oxford, 2004.
[18] J.N. Reddy, D.K. Gartling, The Finite Element Method in Heat Transfer and Fluid Dynamics, second ed., CRC Press, Boca Raton, FL, 2001.
[19] G.E. Karniadakis, S.J. Sherwin, Spectral/*hp* Element Methods for CFD, Oxford University Press, Oxford, 1999.
[20] G.H. Golub, C.F.V. Loan, Matrix Computation, third ed., The Johns Hopkins University Press, Baltimore, MD, 1996.
[21] B.C. Bell, K.S. Surana, A space–time coupled *p*-version least squares finite element formulation for unsteady two-dimensional Navier–Stokes equations, Int. J. Numer. Meth. Eng. 39 (1996) 2593.
[22] W. Couzy, M.O. Deville, A fast Schur complement method for the spectral element discretization of the incompressible Navier–Stokes equations, J. Comput. Phys. 116 (1995) 135.
[23] B.N. Jiang, The Least-Squares Finite Element Method, first ed., Springer, Berlin, 1998.
[24] L.S.G. Kovasznay, Laminar flow behind a two-dimensional grid, Proc. Camb. Philos. Soc. 44 (1948) 58.
[25] Y. Saad, Iterative Methods for Sparse Linear Systems, PWS Publishing Company, Boston, 1996.
[26] M. Kawaguti, P. Jain, Numerical study of a viscous fluid past a circular cylinder, J. Phys. Soc. Jpn. 21 (1966) 2055.
[27] S.C.R. Dennis, G.Z. Chang, Numrical solutions for steady flow past a circular cylinder at Reynolds numbers up to 100, J. Fluid Mech. 42 (1970) 471.
[28] D.J. Tritton, Experiments on the flow past a circular cylinder at low Reynolds numbers, J. Fluid Mech. 6 (1959) 547.
[29] C.L. Chang, J.J. Nelson, Least-squares finite element method for the Stokes problem with zero residual of mass conservation, SIAM J. Numer. Anal. 34 (1997) 480.